

# Border Collision Bifurcations in Two Dimensional Piecewise Smooth Maps

**Soumitro Banerjee\***

Department of Electrical Engineering  
Indian Institute of Technology  
Kharagpur-721302, India  
E-mail: soumitro@ee.iitkgp.ernet.in

and

**Celso Grebogi**

Institute for Plasma Research, Department of Mathematics  
and Institute for Physical Science & Technology  
University of Maryland  
College Park, MD 20742, USA  
E-mail: grebogi@chaos.umd.edu

## Abstract

Recent investigations on the bifurcations in switching circuits have shown that many atypical bifurcations can occur in piecewise smooth maps which can not be classified among the generic cases like saddle-node, pitchfork or Hopf bifurcations occurring in smooth maps. In this paper we first present experimental results to establish the need for the development of a theoretical framework and classification of the new class of bifurcations resulting from border collision. We then present a systematic analysis of such bifurcations by deriving a normal form — the piecewise linear approximation in the neighborhood of the border. We show that there can be eleven qualitatively different types of border collision bifurcations depending on the parameters of the normal form, and these are classified under six cases. We present a partitioning of the parameter space of the normal form showing the regions where different types of bifurcations occur. This theoretical framework will help in explaining bifurcations in all systems which can be represented by two dimensional piecewise smooth maps.

---

\*Corresponding author

# 1 Introduction

Most studies in bifurcation theory have been done using smooth dynamical systems like the Hénon map, the Ikeda map and the pendulum equation. In the class of non-smooth systems, maps with square root singularity have been studied extensively [1, 2, 3, 4] because of their application in impact oscillators and other impacting mechanical systems. On the other hand, piecewise smooth maps with finite one-sided partial derivatives at the discontinuity have attracted relatively little attention. Though the possibility of strange bifurcations like period-2 to period-3 or period-2 to 18-piece chaotic attractor have been reported [5], no systematic study has been made to categorize the possible bifurcations in piecewise smooth maps. Such maps were considered to be just a mathematical possibility as no physical system with these characteristics was known.

However in recent years there has been a discovery that a large class of engineering systems, particularly the switching circuits used in power electronics, yield piecewise smooth maps under discrete modeling, and border collision bifurcations are quite common in such systems [6, 7]. This has provided motivation for the present study whose objective is to systematically analyze all different kinds of bifurcations that can occur in two dimensional piecewise smooth maps.

We consider a general two-dimensional piecewise smooth map  $g(\hat{x}, \hat{y}; \rho)$  which depends on a single parameter  $\rho$ . Let  $\Gamma_\rho$ , given by  $\hat{x} = h(\hat{y}, \rho)$  denote a smooth curve that divides the phase plane into two regions  $R_A$  and  $R_B$ . The map is given by

$$g(\hat{x}, \hat{y}; \rho) = \begin{cases} g_1(\hat{x}, \hat{y}; \rho) & \text{for } \hat{x}, \hat{y} \in R_A, \\ g_2(\hat{x}, \hat{y}; \rho) & \text{for } \hat{x}, \hat{y} \in R_B \end{cases} \quad (1)$$

It is assumed that the functions  $g_1$  and  $g_2$  are both continuous and have continuous derivatives. The map  $g$  is continuous but its derivative is discontinuous at the line  $\Gamma_\rho$ , called the “border”. It is further assumed that the one-sided partial derivatives at the border are finite. We study the bifurcations of this system as the parameter  $\rho$  is varied.

If a bifurcation occurs when the fixed point of the map is in one of the smooth regions  $R_A$  or  $R_B$ , it is one of the generic types, namely, period doubling, saddle-node or Hopf bifurcation. But if a fixed point collides with the borderline, there is a discontinuous jump in the eigenvalue of the Jacobian matrix. In such a case an eigenvalue may not “cross” the unit circle in a smooth way, but rather “jumps” over it as a parameter is varied continuously. One therefore cannot classify the bifurcations arising from such border collisions as those occurring for smooth systems where the eigenvalues cross the unit circle smoothly. In this paper we develop a new classification for border collision bifurcations.

The paper is organized as follows. In Sec. 2, we illustrate the problem with the help of an example of switching circuit. In Sec. 3, the normal form is derived. In Sec. 4, we analyse the border collision bifurcations occurring in piecewise smooth maps. We present a partitioning of the parameter space of the normal form exhibiting various kinds of border collision bifurcations. We conclude in Sec. 5.

## 2 Examples of border collision bifurcations in a power electronic circuit

The subject of power electronics is concerned with high efficiency conversion of electric power, from the form available at the power source, to the form required by the specific appliance or load. Power electronic technology is increasingly finding application in the home and workplace: familiar examples are domestic light dimmers, fluorescent lamp ballasts, battery chargers, and switch-mode power supplies of all electronic appliances including the personal computer.

In contrast with mainstream electronics, power electronics is characterized by the use of electronic *switches* which operate in “on” or “off” state. Since electrical power supplies can be either dc or ac, there are four basic types of power converters: ac-dc, dc-ac, dc-dc and ac-ac. Here we will consider one of the simplest but most useful of power converters — the dc-dc buck converter — which is used to convert a dc input to a dc output at a lower voltage.

The circuit diagram of the buck converter is shown in Fig.1(a). The controlled switch  $S$  (generally realized by a MOSFET) opens and closes in succession, thus “chopping” the dc input into a square wave that alternates between the input voltage  $V_{in}$  and zero. The pulsed waveform is then low-pass filtered by a simple  $LC$  network, removing most of the switching ripple and delivering a relatively smooth dc output voltage  $v$  to the load resistance  $R$ . The diode  $D$  provides a path for the continuation of the inductor current during the *off* period. The dc output voltage can easily be varied by changing the duty ratio, i.e., the fraction of time that the switch is closed in each cycle.

In practice it is necessary to regulate  $v$  against changes in the input voltage and the load current. For example, if a buck converter is used to convert the standard 5 V dc supply used in computers to the 3.3 V needed for the Pentium CPU chip, it would be necessary to regulate the average output voltage at 3.3 V in spite of the varying power demand of the chip. This can be achieved by controlling the switch  $S$  by voltage feedback as shown in Fig.1. In this simple proportional controller, a constant reference voltage  $V_{ref}$  is subtracted from the output voltage and the error is amplified with gain  $A$  to form a control signal  $v_{con} = A(v - V_{ref})$ . The switching signal is generated by comparing the control signal with a periodic sawtooth (ramp) waveform.  $S$  turns on whenever  $v_{con}$  goes below  $v_{ramp}$  and a latch allows it to switch off only at the end of the ramp cycle.

Though this circuit or its variants are used in a large number of practical applications requiring regulated dc power supply, it has been demonstrated [8, 9, 10] that the system can exhibit bifurcations and chaos for a large portion of the parameter space. To investigate the dynamics analytically, we obtain a two dimensional Poincaré map by sampling the inductor current and capacitor voltage at the end of each ramp cycle.

Because of the transcendental form of the equations, the map cannot be determined in closed form. In simulation, the map has to be obtained numerically. It is however possible to infer the form of the map. There are three ways in which the system can move from one observation point to the next: (a) the control voltage is

throughout above the ramp waveform and the switch remains off, (b) the cycle involves an *off* period and an *on* period, (c) the control voltage is throughout below the ramp waveform and the switch remains on. The three cases are shown in Fig.1(b). These are represented by three different expressions of the map. The borderlines are given by the condition where the control voltage grazes the top and bottom of the ramp waveform. Therefore there are three compartments in the phase space, separated by two borderlines, and we have a piecewise smooth map.

We present the experimentally obtained bifurcation diagrams for this system for different sets of parameter values.

An experimental bifurcation diagram is shown in Fig.2(a). Here we find two parameter values (shown with arrows) for which a periodic orbit directly bifurcates into a chaotic orbit. Such bifurcations have been reported earlier in [8, 11, 12, 13]. The slight expansion of the attractor at the bifurcation point is due to system noise and can be ignored in theoretical studies. In Fig.2(b) we present the continuous time plots of  $v_{con}$  and the triangular wave voltage at the bifurcation point shown by the second arrow, where a period-3 orbit bifurcates into a 3-piece chaotic orbit. It is seen that the  $v_{con}$  waveform grazes the top of the triangular wave, which means that a border collision bifurcation has occurred.

The distinguishing feature of this chaotic attractor is that there is no periodic window over a large range of the parameter value. We find from simulation that there are no coexisting attractors in this range. We say a chaotic attractor is *robust* if, for its parameter values there exists a neighborhood in the parameter space with no periodic attractor and the chaotic attractor is unique in that neighborhood [14]. The chaotic attractor resulting from this border collision is therefore robust. The question is, under what condition does robust chaos occur?

Another experimental bifurcation diagram for this system is shown in Fig.3(a). The arrow shows a period doubling bifurcation, but the two bifurcated orbits do not diverge perpendicularly from the path of the fixed point before the critical parameter value. This is therefore not a standard pitchfork bifurcation. This kind of bifurcation has been reported in [15, 16] also. Fig.3(b) gives the continuous time plots of  $v_{con}$  and the triangular wave voltage just after the bifurcation and shows that the period doubling occurred at a border collision. Again the question is, under what condition does this special type of period doubling occur?

It has been reported earlier [17] that this system has coexisting attractors for some ranges of parameter values. Since multiple attractors cannot be seen in experimental bifurcation diagrams, we present a numerically obtained bifurcation diagram in Fig.4 showing the evolution of the main attractor and a coexisting attractor. It is found that the chaotic attractor comes into existence out of nothing at a particular parameter value. Under what condition can such strange bifurcations occur?

In the following sections we develop a complete theory of bifurcations in piecewise smooth maps, from which the answers to the above questions can be derived.

### 3 The normal form

Since the local structure of border collision bifurcations depends only on the local properties of the map in the neighborhood of the border, we study the border collision bifurcations with the help of “normal forms” — the piecewise affine approximations of  $g$  in the neighborhood of the border.

Define

$$\tilde{x} = \hat{x} - h(\hat{y}; \rho), \quad \text{and} \quad \tilde{y} = \hat{y}.$$

This  $\rho$ -dependent change of variables moves the border to the  $\tilde{y}$  axis. Then the map  $g(\hat{x}, \hat{y}; \rho)$  can be written

$$g(\tilde{x} + h(\tilde{y}; \rho), \tilde{y}; \rho) = f(\tilde{x}, \tilde{y}; \rho),$$

and the border is  $\tilde{x} = 0$ . Suppose that when  $\rho = \rho_0$  the map  $f(\tilde{x}, \tilde{y}; \rho)$  has a fixed point  $P_0$  on the border, that is,

$$P_0 = (0, \tilde{y}_0(\rho_0)) = f(0, \tilde{y}_0(\rho_0); \rho_0).$$

Let  $e_1$  be a tangent vector in the  $\tilde{y}$  direction. The vector  $e_1$  maps to a vector  $e_2$ . We assume  $e_2$  is not parallel to  $e_1$ . Define the local coordinates as the following (C.f. Fig. 5). Choose the point  $P_0$  as the new origin for  $e_1$  in the  $\tilde{y}$  direction and  $e_2$  in the  $\tilde{x}$  direction. In these  $\tilde{x}$ - $\tilde{y}$  coordinates, the fixed point  $P_0$  is given by  $(0, 0)$ , and the border  $\Gamma_\rho$  is given by  $\tilde{x} = 0$ . We define the new parameter  $\bar{\mu} = \rho - \rho_0$  so that  $\bar{\mu}_0 = 0$ . Choose the scales such that at  $\bar{\mu} = 0$  a unit vector along  $\tilde{y}$ -axis maps to an unit vector along  $\tilde{x}$ -axis. The phase space is now divided into the two halves  $L$  and  $R$  and the map  $f(\tilde{x}, \tilde{y}; \rho)$  can be written as  $F(\tilde{x}, \tilde{y}, \bar{\mu})$ .

We can write the map  $F(\tilde{x}, \tilde{y}, \bar{\mu})$  in the side  $L$  in the matrix form as

$$F(\tilde{x}, \tilde{y}, \bar{\mu}) = \begin{pmatrix} f_1(\tilde{x}, \tilde{y}; \bar{\mu}) \\ f_2(\tilde{x}, \tilde{y}; \bar{\mu}) \end{pmatrix}, \quad \text{and} \quad F(0, 0; 0) = \begin{pmatrix} 0 \\ 0 \end{pmatrix}.$$

Linearizing  $F(\tilde{x}, \tilde{y}, \bar{\mu})$  in the neighborhood of  $(0, 0; 0)$ , we have:

$$F(\tilde{x}, \tilde{y}, \bar{\mu}) = \begin{pmatrix} J_{11} & J_{12} \\ J_{21} & J_{22} \end{pmatrix} \begin{pmatrix} \tilde{x} \\ \tilde{y} \end{pmatrix} + \bar{\mu} \begin{pmatrix} v_{Lx} \\ v_{Ly} \end{pmatrix} + o(\tilde{x}, \tilde{y}; \bar{\mu}), \quad \text{for } \tilde{x} \leq 0 \quad (2)$$

where

$$\begin{aligned} J_{11} &= \lim_{\tilde{x} \rightarrow 0^-, \tilde{y} \rightarrow 0} \frac{\partial}{\partial \tilde{x}} f_1(\tilde{x}, \tilde{y}; 0), \\ J_{12} &= \lim_{\tilde{x} \rightarrow 0^-, \tilde{y} \rightarrow 0} \frac{\partial}{\partial \tilde{y}} f_1(\tilde{x}, \tilde{y}; 0), \\ J_{21} &= \lim_{\tilde{x} \rightarrow 0^-, \tilde{y} \rightarrow 0} \frac{\partial}{\partial \tilde{x}} f_2(\tilde{x}, \tilde{y}; 0), \\ J_{22} &= \lim_{\tilde{x} \rightarrow 0^-, \tilde{y} \rightarrow 0} \frac{\partial}{\partial \tilde{y}} f_2(\tilde{x}, \tilde{y}; 0), \\ v_{Lx} &= \lim_{\tilde{x} \rightarrow 0^-, \tilde{y} \rightarrow 0} \frac{\partial}{\partial \bar{\mu}} f_1(\tilde{x}, \tilde{y}; 0), \\ v_{Ly} &= \lim_{\tilde{x} \rightarrow 0^-, \tilde{y} \rightarrow 0} \frac{\partial}{\partial \bar{\mu}} f_2(\tilde{x}, \tilde{y}; 0). \end{aligned}$$

The particular choice of coordinates makes  $J_{12} = 1$  and  $J_{22} = 0$ . Further, we note that  $J_{11}$  is the trace (denoted  $\tau_L$ ) and  $J_{21}$  is the negative of the determinant (denoted  $-\delta_L$ ) of the Jacobian matrix. Thus (2) becomes

$$F(\bar{x}, \bar{y}; \bar{\mu}) = \begin{pmatrix} \tau_L & 1 \\ -\delta_L & 0 \end{pmatrix} \begin{pmatrix} \bar{x} \\ \bar{y} \end{pmatrix} + \bar{\mu} \begin{pmatrix} v_{Lx} \\ v_{Ly} \end{pmatrix} + o(\bar{x}, \bar{y}; \bar{\mu}), \quad \text{if } \bar{x} \leq 0, \quad (3)$$

Similarly, for side  $R$  we obtain

$$F(\bar{x}, \bar{y}; \bar{\mu}) = \begin{pmatrix} \tau_R & 1 \\ -\delta_R & 0 \end{pmatrix} \begin{pmatrix} \bar{x} \\ \bar{y} \end{pmatrix} + \bar{\mu} \begin{pmatrix} v_{Rx} \\ v_{Ry} \end{pmatrix} + o(\bar{x}, \bar{y}; \bar{\mu}), \quad \text{if } \bar{x} > 0. \quad (4)$$

where the corresponding quantities in  $R$  are defined in a similar way.

Continuity of the map implies

$$\begin{pmatrix} v_{Lx} \\ v_{Ly} \end{pmatrix} = \begin{pmatrix} v_{Rx} \\ v_{Ry} \end{pmatrix} = \begin{pmatrix} v_x \\ v_y \end{pmatrix}.$$

We now make another change of variables so that the choice of axes is independent of the parameter. The coordinate transformation  $x = \bar{x}$ , and  $y = \bar{y} - \bar{\mu} v_y$ , and  $\mu = \bar{\mu} (v_x + v_y)$  (assuming  $(v_x + v_y) \neq 0$ ) gives

$$G_2(x, y; \mu) = \begin{cases} \begin{pmatrix} \tau_L & 1 \\ -\delta_L & 0 \end{pmatrix} \begin{pmatrix} x \\ y \end{pmatrix} + \mu \begin{pmatrix} 1 \\ 0 \end{pmatrix}, & \text{for } x \leq 0, \\ \begin{pmatrix} \tau_R & 1 \\ -\delta_R & 0 \end{pmatrix} \begin{pmatrix} x \\ y \end{pmatrix} + \mu \begin{pmatrix} 1 \\ 0 \end{pmatrix}, & \text{for } x > 0, \end{cases} \quad (5)$$

which is the desired 2-D normal form.

Note that if  $(v_x + v_y) = 0$ , then the fixed point moves along the border as  $\mu$  varies. Hence we assume the genericity condition  $(v_x + v_y) \neq 0$  to ensure that a border collision occurs at  $\mu = 0$ .

It is interesting to note that  $\tau_L$  and  $\delta_L$  are simply the trace and the determinant of the Jacobian matrix of the fixed point  $P_0$  on  $R_A$  side of the border  $\Gamma$ . Let  $P_\rho$  denote a fixed point of  $g(\hat{x}, \hat{y}; \rho)$  defined on  $\rho_0 - \epsilon < \rho < \rho_0 + \epsilon$  for some small  $\epsilon > 0$ , then  $P_\rho$  depends continuously on  $\rho$ . Assume that  $P_\rho$  is in region  $R_A$  when  $\rho < \rho_0$  and in region  $R_B$  when  $\rho > \rho_0$ , and that  $P_\rho$  is on  $\Gamma$  when  $\rho = \rho_0$ . For  $\rho < \rho_0$ , the eigenvalues of the Jacobian matrix of the fixed point  $P_\rho$  are denoted as  $\lambda_1$  and  $\lambda_2$ . Since the trace and the determinant of the Jacobian is invariant under the transformation of coordinates, we can obtain the values of  $\tau_L$  and  $\delta_L$  as

$$\begin{aligned} \tau_L &= \lim_{\rho \rightarrow \rho_0^-} (\lambda_1 + \lambda_2) \\ \delta_L &= \lim_{\rho \rightarrow \rho_0^-} (\lambda_1 \lambda_2). \end{aligned} \quad (6)$$

The values of  $\tau_R$  and  $\delta_R$  can be calculated in a similar way for  $\rho > \rho_0$ . This property is very important in numerical computations. For a border-crossing periodic orbit

with higher period, we examine the  $p$ th (if the period is  $p$ ) iterate of the map. The matrices in (5) then correspond to the  $p$ th iterate rather than the first iterate of the map.

When  $\delta_L$  and  $\delta_R$  are zero, the system becomes one dimensional and the normal form reduces to

$$G_1(x; \mu) = \begin{cases} a x + \mu & \text{for } x \leq 0, \\ b x + \mu & \text{for } x > 0, \end{cases} \quad (7)$$

where  $a$  and  $b$  are the slopes of the graph at the two sides of the border  $x=0$ .

## 4 Classification of border collision bifurcations

Various combinations of the values of  $\tau_L$ ,  $\tau_R$ ,  $\delta_L$  and  $\delta_R$  exhibit different kinds of bifurcation behaviors as  $\mu$  is varied through zero. To present a complete picture, we break up the four dimensional parameter space into regions with the same qualitative bifurcation phenomena. If the parameter combination is inside a region, then  $g$  and  $G_2$  will have the same types of bifurcations. If it is on a boundary, then higher order terms are needed to determine the bifurcations of  $g$ .

The fixed points of the system in both sides of the boundary are given by

$$\begin{aligned} L^* &= \left( \frac{\mu}{1 - \tau_L + \delta_L}, \frac{-\delta_L \mu}{1 - \tau_L + \delta_L} \right) \\ R^* &= \left( \frac{\mu}{1 - \tau_R + \delta_R}, \frac{-\delta_R \mu}{1 - \tau_R + \delta_R} \right) \end{aligned}$$

and the stability of each of them is determined by the eigenvalues  $\lambda_{1,2} = \frac{1}{2} (\tau \pm \sqrt{\tau^2 - 4\delta})$ . If the eigenvalues are real, the slopes of the corresponding eigenvectors are given by  $-(\delta/\lambda_1)$  and  $-(\delta/\lambda_2)$ , respectively. Since we consider only dissipative systems, we assume  $|\delta_L| < 1$  and  $|\delta_R| < 1$ . Under this condition there can be four types of fixed points.

1. When  $\delta > \tau^2/4$ , both eigenvalues of the Jacobian are complex, indicating that the fixed point is spirally attracting. If  $\tau > 0$ , it is a clockwise spiral, and if  $\tau < 0$  the spiralling motion is counter-clockwise.
2. When  $\delta < \tau^2/4$ , both eigenvalues are real. If  $2\sqrt{\delta} < \tau < (1 + \delta)$  then the eigenvalues are positive and the fixed point is a regular attractor. If  $-2\sqrt{\delta} > \tau > -(1 + \delta)$  then the eigenvalues are negative and it is a flip attractor.
3. If  $\delta < \tau - 1$  and  $0 < \delta < 1$ , then  $0 < \lambda_2 < 1$  and  $\lambda_1 > 1$ ; if  $\delta < \tau - 1$  and  $-1 < \delta < 0$ , then  $-1 < \lambda_2 < 0$  and  $\lambda_1 > 1$ . The fixed point is a regular saddle in both cases.
4. If  $\delta < -\tau - 1$  and  $0 < \delta < 1$ , then  $\lambda_2 < -1$  and  $-1 < \lambda_1 < 0$ ; if  $\delta < -\tau - 1$  and  $-1 < \delta < 0$ , then  $\lambda_2 < -1$  and  $0 < \lambda_1 < 1$ . The fixed point is a flip saddle for both cases.

When referring to sides  $L$  and  $R$ , these quantities have the appropriate subscripts, i.e.,  $\lambda_{1L}$ ,  $\lambda_{2L}$  are the eigenvalues in side  $L$  and  $\lambda_{1R}$ ,  $\lambda_{2R}$  are the eigenvalues in side  $R$ . As a fixed point collides with the border, its character can change from any one of the above types to any other. This provides a way of classifying border collision bifurcations.

It may be noted that in some portions of the parameter space there may be no fixed point in half of the phase space. For example, the location of  $L^*$  calculated by the above formula may turn out to be in side  $R$ . In such cases, the dynamics in  $L$  is determined by the character of the “virtual” fixed point. We denote such virtual fixed points by the overbar sign, as  $\bar{L}^*$  and  $\bar{R}^*$ . If the eigenvalues are real, invariant manifolds of these virtual fixed points still exist and play an important role in deciding the system dynamics.

It should also be noted that if a certain kind of bifurcation occurs when  $\mu$  is increased through zero, the same kind of bifurcation would also occur when  $\mu$  is decreased through zero if the parameters in  $L$  and  $R$  are interchanged. Therefore, there exists a symmetry in the parameter space and in the following discussion it suffices to describe the bifurcations in half the parameter space. Moreover, we first consider the case of positive determinant, which constitute a large class of physical systems. We take up the special features of systems with negative determinant at a later stage.

A special feature of the normal form (5) is that the unstable manifolds fold at every intersection with the x-axis, and the images of every fold point is a fold point. The stable manifolds fold at every intersection with the y-axis and the pre-image of every fold point is a fold point. The argument is as follows. Forward iterate of points on the unstable manifold remain on the same manifold. In the normal form, points on the y-axis map to points on the x-axis. As an unstable manifold crosses the y-axis, one linear map changes to another linear map. Therefore the slope of the unstable manifold in the two sides of the x-axis cannot be the same unless the parameters of the normal form in the two sides of the border are the same (implying a smooth map). In case of the stable manifold, the same argument applies for the inverse map. The inverse map of the normal form is given by

$$G_2^{-1}(x, y; \mu) = \begin{cases} \begin{pmatrix} 0 & -\frac{1}{\delta_L} \\ 1 & \frac{\tau_L}{\delta_L} \end{pmatrix} \begin{pmatrix} x \\ y \end{pmatrix} + \mu \begin{pmatrix} 0 \\ -1 \end{pmatrix}, & \text{for } y > 0, \\ \begin{pmatrix} 0 & -\frac{1}{\delta_R} \\ 1 & \frac{\tau_R}{\delta_R} \end{pmatrix} \begin{pmatrix} x \\ y \end{pmatrix} + \mu \begin{pmatrix} 0 \\ -1 \end{pmatrix}, & \text{for } y \leq 0. \end{cases} \quad (8)$$

Since its borderline is along the x-axis, and points on the x-axis map to points on the y-axis, we conclude that the stable manifold must have different slopes in the two sides of the y-axis.

We now present the partitioning of the parameter space as shown in Fig.6. The system behavior in the various regions of the parameter space are taken up in the following subsections.

## 4.1 Border collision pair bifurcation

**Case 1:** If

$$\tau_L > (1 + \delta_L) \quad \text{and} \quad \tau_R < (1 + \delta_R), \quad (9)$$

then there is no fixed point for  $\mu < 0$  and there are two fixed points, one each in  $L$  and  $R$ , for  $\mu > 0$ . The two fixed points are born on the border at  $\mu = 0$ . We call this a *border collision pair* bifurcation. An analogous situation occurs if  $\tau_L < (1 + \delta_L)$  and  $\tau_R > (1 + \delta_R)$  as  $\mu$  is reduced through zero. Due to the symmetry of the two cases, we consider only the parameter region (9). There can be three types of border collision pair bifurcations depending on the character of the orbits for  $\mu > 0$ .

**Case 1(a):** If  $(1 + \delta_R) > \tau_R > -(1 + \delta_R)$ , then  $R^*$  is stable. Therefore it is like a saddle-node bifurcation, where a periodic attractor appears at  $\mu = 0$ . There are two special features of this saddle node bifurcation. First, the fixed points are born on the border and move away from it as  $\mu$  is increased. Second, there is no intermittency associated with this bifurcation.

**Case 1(b):** If

$$\tau_L > (1 + \delta_L) \quad \text{and} \quad \tau_R < -(1 + \delta_R) \quad \text{and} \quad (10)$$

$$\delta_L \tau_R \lambda_{1L} - \delta_R \lambda_{1L} \lambda_{2L} + \delta_R \lambda_{2L} - \delta_L \tau_R + \tau_L \delta_L - \delta_L^2 - \lambda_{2L} \delta_L > 0 \quad (11)$$

there is a bifurcation from no attractor to a chaotic attractor. The chaotic attractor for  $\mu > 0$  is robust [14].

**Case 1(c):** If  $\tau_L > (1 + \delta_L)$  and  $\tau_R < -(1 + \delta_R)$  and

$$\delta_L \tau_R \lambda_{1L} - \delta_R \lambda_{1L} \lambda_{2L} + \delta_R \lambda_{2L} - \delta_L \tau_R + \tau_L \delta_L - \delta_L^2 - \lambda_{2L} \delta_L \leq 0$$

then there is an unstable chaotic orbit for  $\mu > 0$ .

For (10),  $L^*$  is a regular saddle and  $R^*$  is a flip saddle. Let  $\mathbf{U}_L$  and  $\mathbf{S}_L$  be the unstable and stable manifolds of  $L^*$  and  $\mathbf{U}_R$  and  $\mathbf{S}_R$  be the unstable and stable manifolds of  $R^*$ , respectively. As shown earlier,  $\mathbf{U}_L$  and  $\mathbf{U}_R$  experience folds along the x-axis, and all images of fold points are fold points.  $\mathbf{S}_L$  and  $\mathbf{S}_R$  fold along the y-axis, and all pre-images of fold points are fold points.

For condition (10),  $\lambda_{1L} > \lambda_{2L} > 0$  and  $0 > \lambda_{1R} > \lambda_{2R}$ . The stable eigenvector at  $R^*$  has a slope  $m_1 = (-\delta_R/\lambda_{1R})$  and the unstable eigenvector has a slope  $m_2 = (-\delta_R/\lambda_{2R})$ . Since points on an eigenvector map to points on the same eigenvector and since points on the y-axis map to the x-axis, we conclude that points of  $\mathbf{U}_R$  to the left of y-axis map to points above x-axis. From this we find that  $\mathbf{U}_R$  has an angle  $m_3 = (\delta_L \lambda_{2R})/(\delta_R - \tau_L \lambda_{2R})$  after the first fold. Under condition (10) we have  $m_1 > m_2 > 0$  and  $m_3 < 0$ . Therefore there must be a transverse homoclinic intersection in  $R$ . This implies an infinity of homoclinic intersections and the existence of a chaotic orbit.

We now investigate the stability of this orbit. The basin boundary is formed by  $\mathbf{S}_L$ .  $\mathbf{S}_L$  folds at the y-axis and intersects the x-axis at point  $C$ . The portion of  $\mathbf{U}_L$  to the left of  $L^*$  goes to infinity and the portion to the right of  $L^*$  leads to the chaotic

orbit.  $\mathbf{U}_L$  meets the x-axis at point  $D$ , and then undergoes repeated foldings leading to an intricately folded compact structure as shown in Fig.7.

The unstable eigenvector at  $L^*$  has a negative slope given by  $(-\delta_L/\lambda_{1L})$ . Therefore it must have a heteroclinic intersection with  $\mathbf{S}_R$ . Since both  $\mathbf{U}_L$  and  $\mathbf{U}_R$  have transverse intersections with  $\mathbf{S}_R$ , by the Lambda Lemma [18] we conclude that for each point  $q$  on  $\mathbf{U}_R$  and for each  $\epsilon$ -neighborhood  $N_\epsilon(q)$ , there exist points of  $\mathbf{U}_L$  in  $N_\epsilon(q)$ . Since  $\mathbf{U}_L$  comes arbitrarily close to  $\mathbf{U}_R$ , the attractor must span  $\mathbf{U}_L$  in one side of the heteroclinic point.

Since all initial conditions in  $L$  converge on  $\mathbf{U}_L$  and all initial conditions in  $R$  converge on  $\mathbf{U}_R$ , and since there are points of  $\mathbf{U}_L$  in every neighborhood of  $\mathbf{U}_R$ , we conclude that the attractor is unique. This chaotic attractor cannot be destroyed by small changes in the parameters. Since small changes in the parameters can only cause small changes in the Lyapunov exponents, where the chaotic attractor is stable, it is also robust.

It is clear from this geometrical structure that no point of the attractor can be to the right of point  $D$ . If  $D$  lies towards the left of  $C$ , the chaotic orbit is stable. If  $D$  falls outside the basin of attraction, it is an unstable chaotic orbit or chaotic saddle. From this, the condition (11) of stability of the chaotic attractor is obtained. If  $\delta_L = \delta_R = \delta$  this condition reduces to  $\tau_R \lambda_{1L} - \lambda_{1L} \lambda_{2L} + \tau_L - \tau_R - \delta > 0$ .

## 4.2 Border crossing bifurcations

In all regions of the parameter space except (9), a fixed point crosses the border as  $\mu$  is varied through zero. The resulting bifurcations are called *border crossing* bifurcations. In the following discussions we consider the bifurcations as  $\mu$  varies from a negative value to a positive value.

**Case 2:** *Linear attractor to flip saddle.* This occurs

$$\text{if } 2\sqrt{\delta_L} < \tau_L < (1 + \delta_L) \text{ and } \tau_R < -(1 + \delta_R).$$

There is a bifurcation from a period-1 attractor to a chaotic attractor as  $\mu$  is increased through zero. This chaotic attractor is robust.

For  $\mu < 0$ ,  $L^*$  is a linear attractor while  $\bar{R}^*$  is a flip saddle. All initial conditions in  $L$  converge on to  $L^*$ , while initial conditions in  $R$  converge on to  $\mathbf{U}_R$ . Since  $\mathbf{U}_R$  must have a heteroclinic intersection with one of the stable manifolds of  $L$ , all initial conditions in  $R$  also converge on to  $L^*$ .

For  $\mu > 0$ ,  $R^*$  is a flip saddle. As shown in the discussion for Case 1(b), there is a homoclinic intersection in  $R$  implying the existence of a chaotic orbit. As  $\bar{L}^*$  is in  $R$ , its stable manifolds point towards  $R$ . Since there is an intersection of  $\mathbf{S}_R$  with the invariant manifold associated with  $\lambda_{1L}$ , all initial conditions converge on  $\mathbf{U}_R$ , making the chaotic attractor unique.

**Case 3:** There is a unique period-1 attractor for both positive and negative values of  $\mu$  in the following cases. At border collision, only the path of the fixed point changes.

*Regular attractor to spiral attractor:* This occurs

$$\text{if } 2\sqrt{\delta_L} < \tau_L < (1 + \delta_L) \text{ and } -2\sqrt{\delta_R} < \tau_R < 2\sqrt{\delta_R}.$$

For  $\mu < 0$ , all initial conditions in  $R$  are attracted to  $\bar{R}^*$  which is in  $L$ . All initial conditions in  $L$  converge on to  $L^*$ . Therefore the fixed point is the unique attractor. For  $\mu > 0$ , all initial conditions in  $L$  move linearly towards  $\bar{L}^*$  which is in  $R$ , and all points in  $R$  spiral towards  $R^*$ . Therefore  $R^*$  is the unique attractor.

*Spiral attractor to spiral attractor having the same sense of rotation:* This occurs

$$\begin{aligned} \text{if } & 0 < \tau_L < 2\sqrt{\delta_L} \text{ and } 0 < \tau_R < 2\sqrt{\delta_R} \\ \text{or } & -2\sqrt{\delta_L} < \tau_L < 0 \text{ and } -2\sqrt{\delta_R} < \tau_R < 0. \end{aligned}$$

If the spiralling orbits in  $L$  and  $R$  have the same sense, there is an overall spiralling orbit converging on the fixed point. Therefore there is a unique period-1 attractor for both  $\mu < 0$  and  $\mu > 0$ .

*Regular attractor to regular attractor:*

$$2\sqrt{\delta_L} < \tau_L < (1 + \delta_L) \text{ and } 2\sqrt{\delta_R} < \tau_R < (1 + \delta_R),$$

*Flip attractor to flip attractor:*

$$-2\sqrt{\delta_L} > \tau_L > -(1 + \delta_L) \text{ and } -2\sqrt{\delta_R} > \tau_R > -(1 + \delta_R),$$

*Regular attractor to flip attractor:*

$$2\sqrt{\delta_L} < \tau_L < (1 + \delta_L) \text{ and } -2\sqrt{\delta_R} > \tau_R > -(1 + \delta_R).$$

In the above three cases, for  $\mu < 0$ , initial conditions in  $R$  move linearly to  $\bar{R}^*$ . Since there must be a heteroclinic intersection of the stable manifolds, all initial conditions converge on  $L^*$ . The situation for  $\mu > 0$  is similar.

**Case 4:** In the following cases there can be bifurcation from multiple attractors to multiple attractors. There are general mechanisms for the occurrence of coexisting attractors.

*Spiral attractor to spiral attractor with opposite sense of rotation:* This occurs

$$\begin{aligned} \text{if } & 0 < \tau_L < 2\sqrt{\delta_L} \text{ and } -2\sqrt{\delta_R} < \tau_R < 0 \\ \text{or } & -2\sqrt{\delta_L} < \tau_L < 0 \text{ and } 0 < \tau_R < 2\sqrt{\delta_R}. \end{aligned}$$

*Spiral attractor to flip attractor:* This occurs

$$\text{if } -2\sqrt{\delta_L} < \tau_L < 2\sqrt{\delta_L} \text{ and } -2\sqrt{\delta_R} > \tau_R > -(1 + \delta_R).$$

There can be multiple attractors on both sides of  $\mu$ , one of which is a fixed point.

**Case 5:** In the parameter space region

$$\tau_R < -(1 + \delta_R) \text{ and } \tau_L < 0,$$

initial conditions in  $L$  move to  $R$  and vice versa. Therefore the dynamics is governed by the stability of the second iterate with one point in  $L$  and the other in  $R$ .

The eigenvalues of the second iterate are

$$\frac{1}{2} \left( \tau_L \tau_R - \delta_R - \delta_L \pm \sqrt{\tau_L^2 \tau_R^2 - 2\tau_L \tau_R \delta_R - 2\tau_L \delta_L \tau_R + \delta_R^2 - 2\delta_R \delta_L + \delta_L^2} \right)$$

From this, the condition of stability of the period-2 orbit is obtained as

$$1 - \tau_L \tau_R + \delta_L + \delta_R + \delta_L \delta_R > 0 \quad (12)$$

There are three sub-cases:

**Case 5(a):** If

$$\begin{aligned} \tau_R < -(1 + \delta_R) \quad \text{and} \quad \tau_L < -2\sqrt{\delta_L} \\ \text{and} \quad 1 - \tau_L \tau_R + \delta_L + \delta_R + \delta_L \delta_R > 0, \end{aligned}$$

then there is a unique period-1 attractor for  $\mu < 0$  and a unique period-2 attractor for  $\mu > 0$ .

For  $\mu < 0$ ,  $L^*$  is a flip attractor and  $\bar{R}^*$  is a flip saddle. All initial conditions in  $L$  converge on  $L^*$  and all initial conditions in  $R$  go to  $L$  in the first iteration and then converge on to  $L^*$ . For  $\mu > 0$ , the condition (12) ensures the stability of the period-2 orbit. The existence of heteroclinic intersection makes the attractor unique.

This is like a period doubling bifurcation occurring on the borderline. In contrast with standard period doubling bifurcation, the distinctive feature of the border collision period doubling is that as  $\mu$  is varied through zero, the bifurcated orbit does not emerge orthogonally from the orbit before the bifurcation.

**Case 5(b):** If

$$\begin{aligned} \tau_R < -(1 + \delta_R) \quad \text{and} \quad -2\sqrt{\delta_L} < \tau_L < 0 \\ \text{and} \quad 1 - \tau_L \tau_R + \delta_L + \delta_R + \delta_L \delta_R > 0, \end{aligned}$$

then for  $\mu < 0$  there can be multiple attractors one of which is a period-1 fixed point. For  $\mu > 0$ , the period-2 orbit involving both  $L$  and  $R$  is stable. Therefore there is an unique period-2 attractor.

**Case 5(c):** If

$$\begin{aligned} \tau_R < -(1 + \delta_R) \quad \text{and} \quad -(1 + \delta_L) < \tau_L \\ \text{and} \quad 1 - \tau_L \tau_R + \delta_L + \delta_R + \delta_L \delta_R < 0, \end{aligned}$$

then there is a period-1 attractor for  $\mu < 0$ . For  $\mu > 0$ , since (12) is not satisfied, it implies that the fixed point of the twice iterated map is unstable. If the eigenvalues are real, initial conditions diverge away from it along the unstable eigenvector and if they are complex, initial conditions diverge spirally. Therefore there can be no attractor for  $\mu > 0$ .

**Case 5(d):** If

$$\tau_L < -(1 + \delta_L) \quad \text{and} \quad \tau_R < -(1 + \delta_R),$$

there is no attractor for both positive and negative values of  $\mu$  since all the fixed points of the first and second iterate are unstable.

**Case 6:** *Spiral attractor to flip saddle:* This occurs

$$\text{if } 0 < \tau_L < 2\sqrt{\delta_L} \quad \text{and} \quad \tau_R < -(1 + \delta_R).$$

For  $\mu < 0$ , there can be multiple attractors one of which is a period-1 fixed point. The asymptotic behavior for  $\mu > 0$  may be a periodic attractor (of periodicity greater than unity), or chaotic attractor. There is no mechanism to prevent the occurrence of multiple attractors.

This gives a complete description of the bifurcations that can occur at various regions of the parameter space of the normal form (5). Representative bifurcation diagrams of the cases (where attractors exist) are shown in Fig.8.

### 4.3 The case of negative determinant

If the determinant is negative, one has to find out which type of fixed point changes to which type at it moves across the border. Depending on the type of the fixed point at the two sides of the border, the bifurcations will be of the same kind as discussed in the previous section. For example, if  $\delta_L, \delta_R < 0$  then the eigenvalues are real for all values of  $\tau_L$  and  $\tau_R$ . Therefore there can be no coexisting attractors anywhere in the parameter space.

There is however a difference in the equation for the boundary between the regions of Case 1(b) and Case 1(c). For  $-1 < \delta_R < 0$ , we have  $1 > \lambda_{1R} > 0$ ,  $\lambda_{2R} < -1$ , and  $R^*$  is located above the x-axis. A positive value of  $\lambda_{1R}$  implies that  $\mathbf{U}_L$  converges on  $\mathbf{U}_R$  from one side. If

$$\frac{\lambda_{1L} - 1}{\tau_L - 1 - \delta_L} > \frac{\lambda_{2R} - 1}{\tau_R - 1 - \delta_R} \quad (13)$$

then the intersection of  $\mathbf{U}_L$  with the x-axis remains the rightmost point of the attractor and (11) still gives the parameter range for boundary crisis. But if (13) is not satisfied, the intersection of  $\mathbf{U}_R$  with the x-axis becomes the rightmost point of the attractor, and the condition of existence of the chaotic attractor changes to

$$\frac{\lambda_{2R} - 1}{\tau_R - 1 - \delta_R} < \frac{\delta_L (\tau_L - \delta_L - \lambda_{2L})}{(\tau_L - 1 - \delta_L) (\delta_R \lambda_{2L} - \delta_L \tau_R)} \quad (14)$$

For  $\delta_L < 0$  and  $\delta_R < 0$ ,  $L^*$  is below the x-axis and the same logic as above applies. But if  $\delta_L < 0$  and  $\delta_R > 0$ , the stable manifold of  $R^*$  has a negative eigenvalue and hence  $\mathbf{U}_L$  does not approach  $\mathbf{U}_R$  from one side. Therefore, if (13) is not satisfied, there is no analytic condition for boundary crisis — it has to be determined numerically.

## 5 Conclusions

In this paper we have investigated the various types of border collision bifurcations that can occur in piecewise smooth maps by deriving a piecewise affine approximation of the map in the neighborhood of the border. We have shown that there can be basically eleven different types of border collision bifurcations, classified under six “cases”. We have presented a partitioning of the parameter space into regions where qualitatively different bifurcations occur.

This body of knowledge helps us in explaining the bifurcations observed in experimental and numerical investigations of switching circuits, some of which have been

presented in Sec.2. For example, the experimental bifurcations of the type seen in Fig.2 can occur in Case 2 and a part of Case 6. A period doubling bifurcation of the type shown in Fig.3 can occur in the second iterate of the map if the parameters fall under Cases 5(a), 5(b) and a part of Case 6 (coexisting attractors can not be observed in experimental bifurcation diagrams). The sudden appearance of a chaotic attractor as in Fig.4 can occur in border collision pair bifurcation and can be categorized under Case 1(b). Note that this bifurcation occurs in the third iterate while the period-1 attractor is present, and therefore the resulting chaotic attractor is not robust.

The theoretical problem dealt in this paper was posed by the recent investigations in switching electrical circuits. But we believe that such atypical bifurcations will be observed in other nonsmooth physical systems also and the theory developed in this paper will help in understanding the nonlinear phenomena and bifurcations in such systems.

## Acknowledgements

We acknowledge the discussions with Prof. J. A. Yorke and Dr. G. H. Yuan in the initial stages of this work. This work was partly supported by NSF-CNPq, USA and by III 4(23)/94-ET, DST, India.

## References

- [1] W. Chin, E. Ott, H. E. Nusse, and C. Grebogi, *Physical Review E*, 50(6):4427–4444, 1994.
- [2] W. Chin, E. Ott, H. E. Nusse, and C. Grebogi, *Physics Letters A*, 201:197–204, 1995.
- [3] E. H. Nusse, E. Ott, and J. A. Yorke, *Physical Review E*, 49:1073–1076, 1994.
- [4] C. Budd and F. Dux. *Phil. Trans. R. Soc. Lond. A*, 347:365–389, 1994.
- [5] E. H. Nusse and J. A. Yorke, *Physica D*, 57:39–57, 1992.
- [6] S. Banerjee, E. Ott, J. A. Yorke, and G. H. Yuan, In *IEEE Power Electronics Specialists' Conference*, pages 1337–1344, 1997.
- [7] G. H. Yuan, S. Banerjee, E. Ott, and J. A. Yorke, *IEEE Transactions on Circuits & Systems-I: Fundamental Theory & Applications*, 45(7):707–716, 1998.
- [8] J. H. B. Deane and D. C. Hamill, *IEEE Transactions on Power Electronics*, 5(3):260–268, 1990.
- [9] D. C. Hamill, In *Nonlinear dynamics of electronic systems*, Dublin, 1995.
- [10] D. C. Hamill and J. H. B. Deane, *IEEE Transactions on Power Electronics*, 7(1):25–36, 1992.
- [11] C. K. Tse and W. C. Y. Chan, In *Power Electronics Specialists' Conference*, 1995.

- [12] M. Ohnishi and N. Inaba, *IEEE Transactions on Circuits and Systems-I: Fundamental Theory and Applications*, 41(6):433–442, 1994.
- [13] I. Zafrany and S. Ben-Yaakov. In *Power Electronics Specialists' Conference*, pages 1111–1117, 1995.
- [14] S. Banerjee, J. A. Yorke, and C. Grebogi, *Physical Review Letters*, 80:3049–3052, 1998.
- [15] J. H. B. Deane, *IEEE Transactions on circuits and systems-1 : fundamental and applications*, 39(8):680–683, 1992.
- [16] W. C. Y. Chan and C. K. Tse, In *Power Electronics Specialists' Conference*, pages 789–795, 1996.
- [17] S. Banerjee, *IEEE Transactions on Circuits and Systems-I: Fundamental Theory and Applications*, 44(9):847–849, 1997.
- [18] K. T. Alligood, T. D. Sauer, and J. A. Yorke, *Chaos: an introduction to dynamical systems*. Springer, 1996.

### Figure captions

Figure 1: (a) The buck converter with duty cycle controlled by voltage feedback, (b) The three ways the state can move from one sampling instant to the next.

Figure 2: Experimental bifurcation diagram of the buck converter. The parameter values are:  $R = 23.5\Omega$ ,  $C = 5\mu\text{F}$ ,  $L = 2.96\text{mH}$ , triangular wave:  $V_U = 8.43\text{V}$ ,  $V_L = 3.62\text{V}$ , frequency 12 kHz. Bifurcation parameter  $V_{in}$  varied from 35 to 75 V.

Figure 3: Experimental bifurcation diagram of the buck converter. The parameter values are:  $R = 28.9\Omega$ ,  $C = 5\mu\text{F}$ ,  $L = 2.96\text{mH}$ , triangular wave:  $V_U = 8.43\text{V}$ ,  $V_L = 3.62\text{V}$ , frequency 8 kHz. Bifurcation parameter  $V_{in}$  varied from 50 to 70 V.

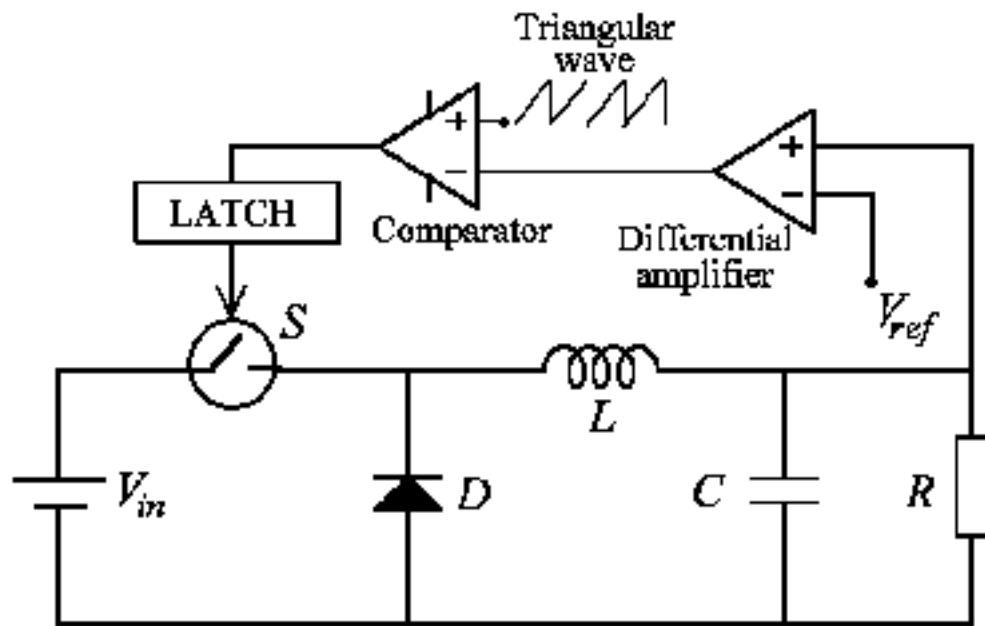
Figure 4: Numerically obtained bifurcation diagram of the buck converter. The parameter values are:  $R = 22\Omega$ ,  $C = 47\mu\text{F}$ ,  $L = 20\text{mH}$ , triangular wave:  $V_U = 8.2\text{V}$ ,  $V_L = 3.8\text{V}$ , time period  $400\mu\text{s}$ .

Figure 5: The transformation of coordinates from the two dimensional piecewise smooth map to the normal form.

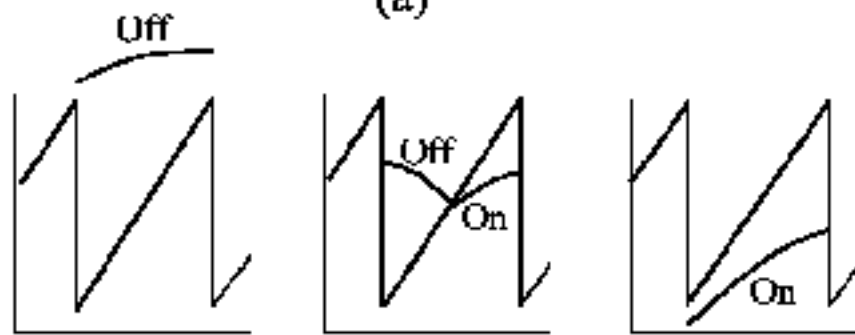
Figure 6: The partitioning of the parameter space into regions with the same qualitative bifurcation phenomena. The numbering of the regions are the cases as discussed in the text. The regions shown in primed numbers have the same bifurcation behavior as the unprimed ones when  $\mu$  is varied in the opposite direction.

Figure 7: The stable and unstable manifolds of  $L^*$  for  $\tau_L = 1.7$ ,  $\delta_L = 0.5$ ,  $\tau_R = -1.7$ ,  $\delta_R = 0.5$ .  $R^*$  is marked by the small cross inside the attractor.

Figure 8: Representative bifurcation diagrams of the normal form when  $\mu$  is varied from a negative value to a positive value. For the cases where multiple attractors can exist, only one of many possibilities is shown. *Case 1(a)*: No attractor to period-1 attractor; *Case 1(b)*: No attractor to chaos; *Case 2*: Period-1 to chaos; *Case 3*: Period-1 to period-1; *Case 4*: Period-1 + period-3 coexisting attractors to period-1 + period-4 coexisting attractors; *Case 5(a)*: Period-1 to period-2; *Case 5(b)*: Period-1 + period-11 coexisting attractors to period-2 attractor; *Case 6*: Period-1 to coexisting period-5 + chaotic attractors.



(a)



(b)

Fig.1



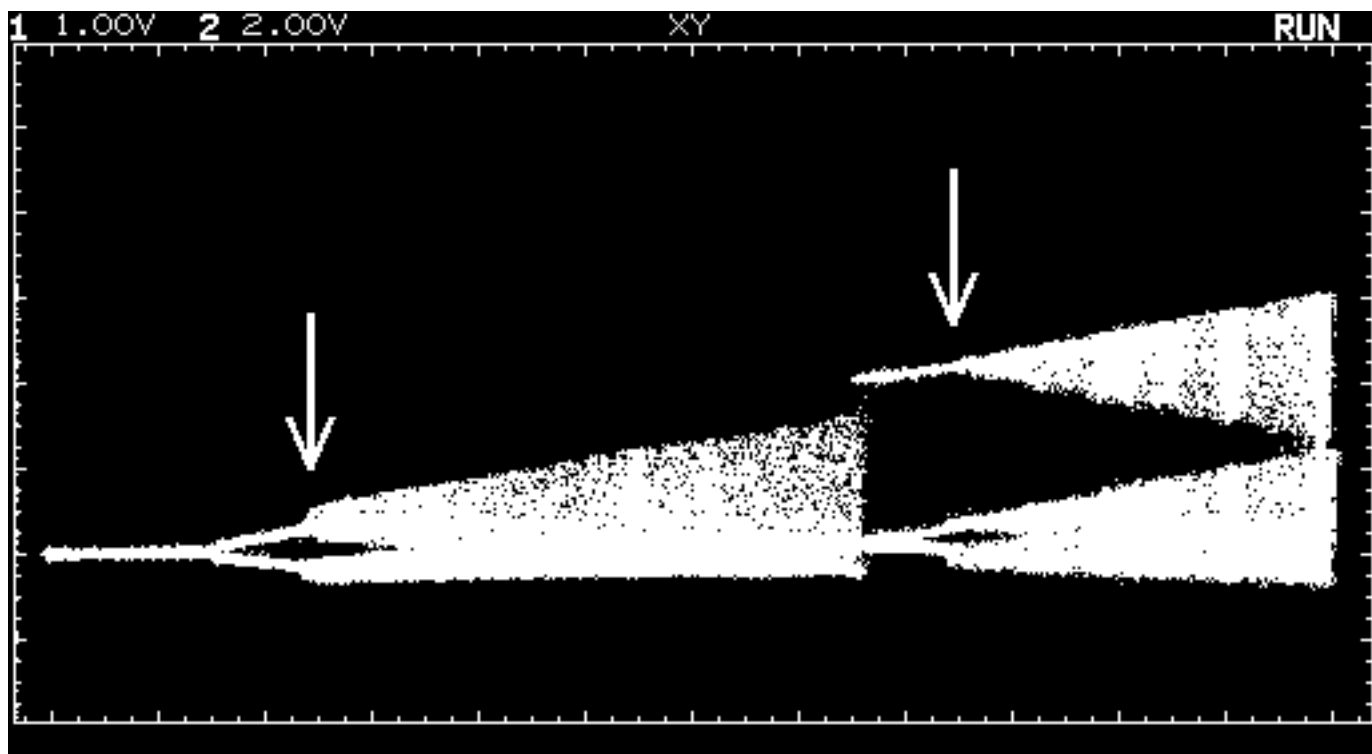


Fig.2(a)



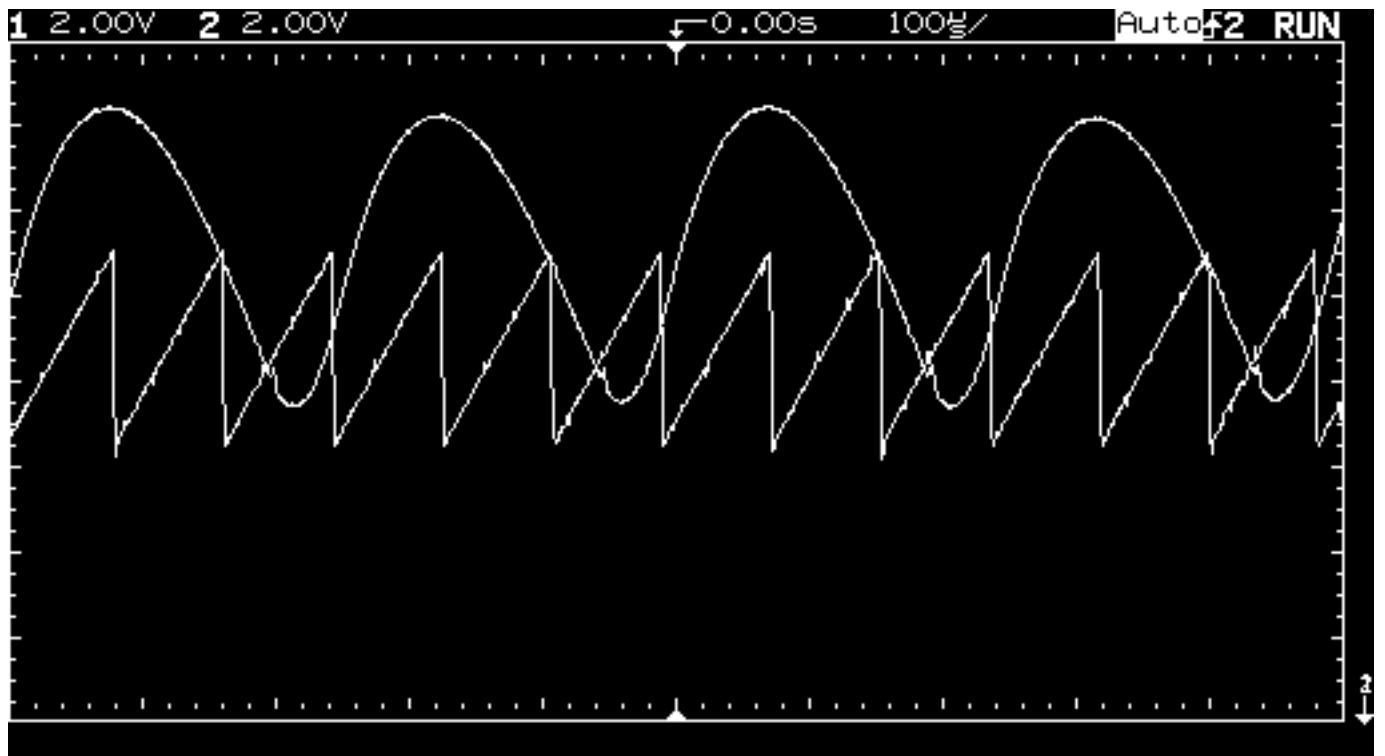


Fig.2(b)



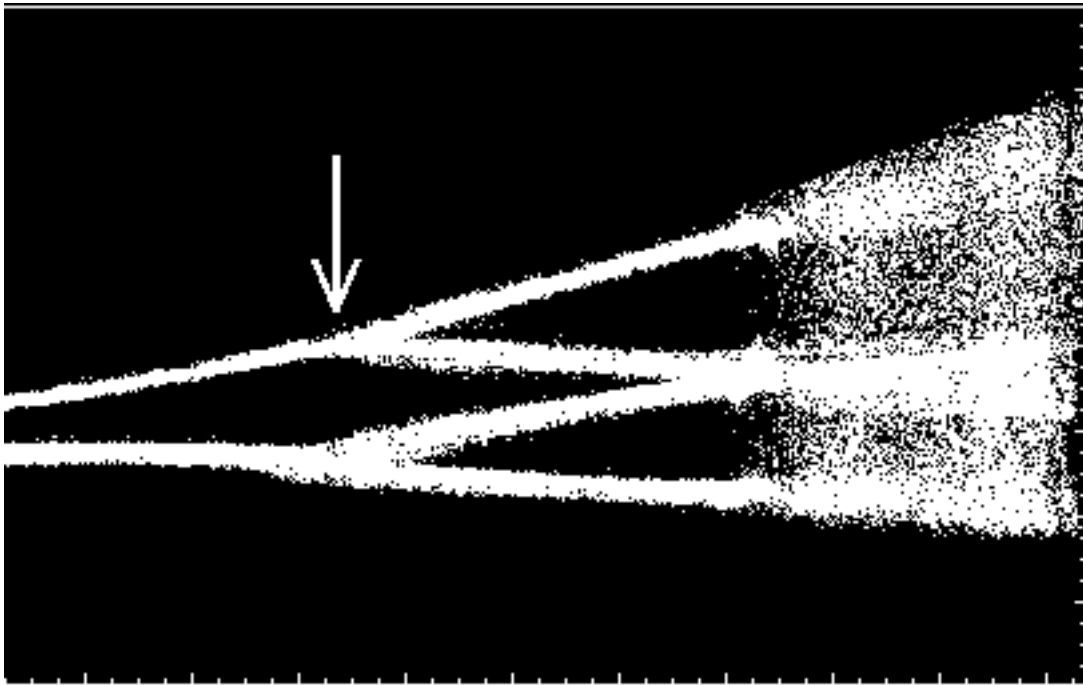
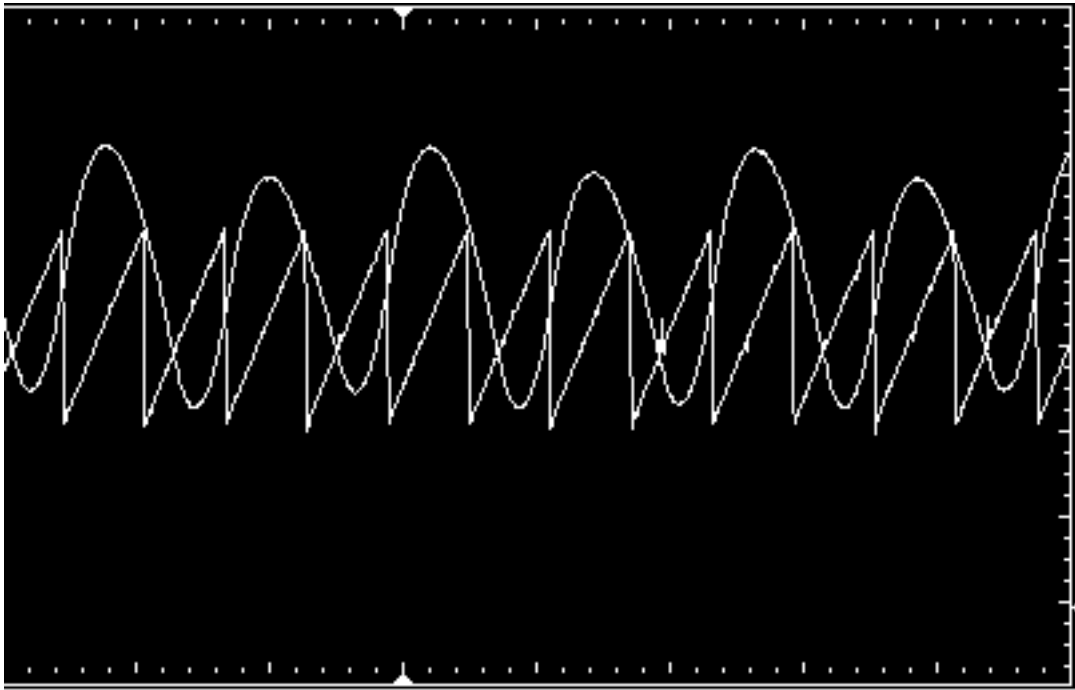


Fig.3(a)





**Fig.3(b)**



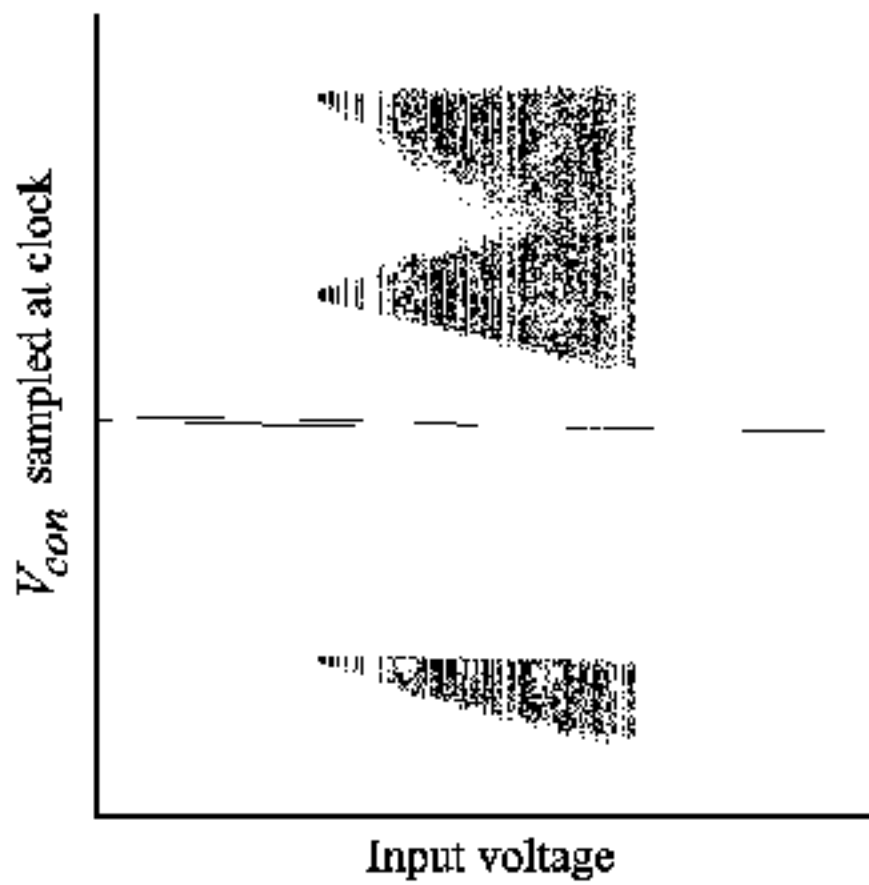


Fig.4



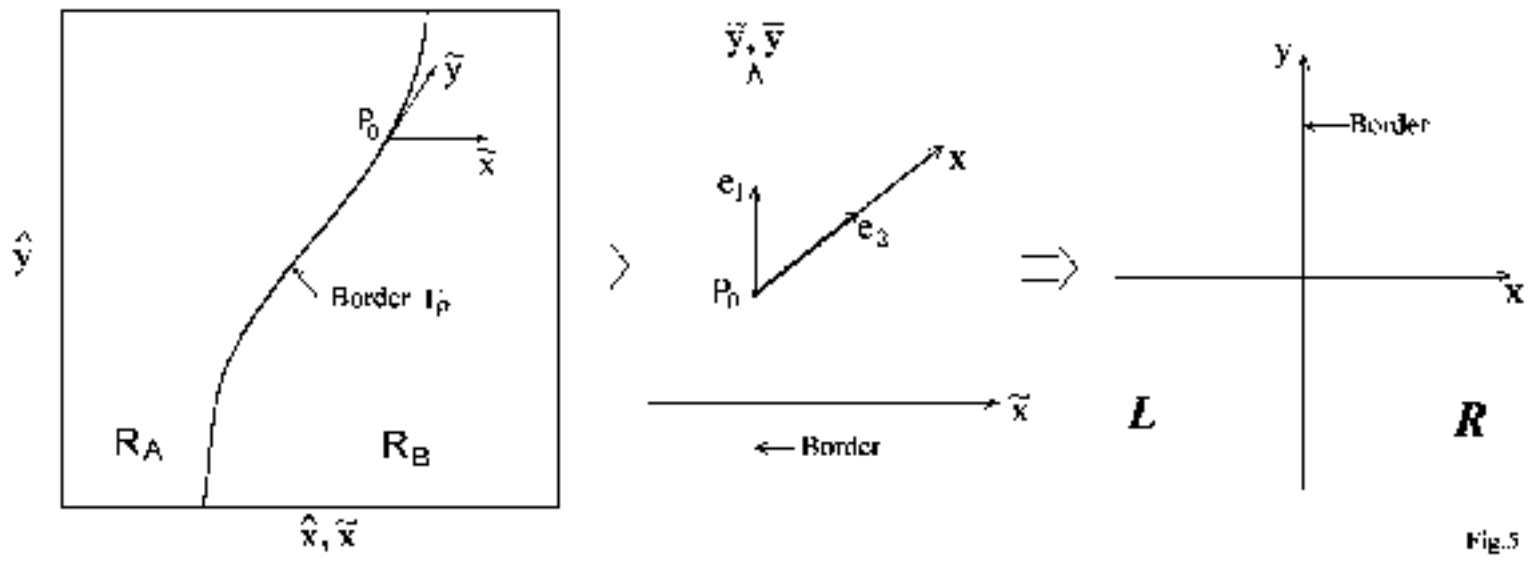


Fig.5



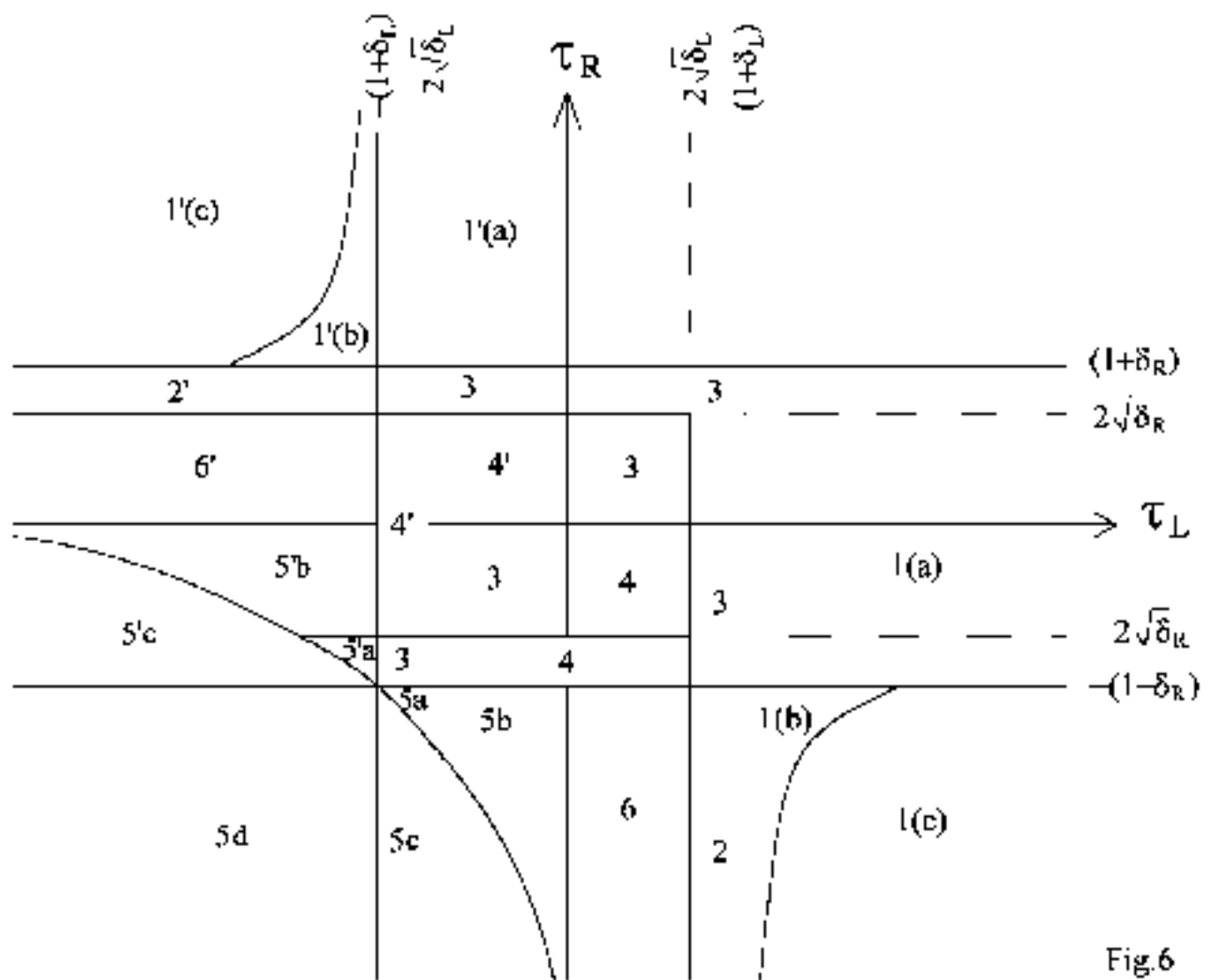


Fig.6



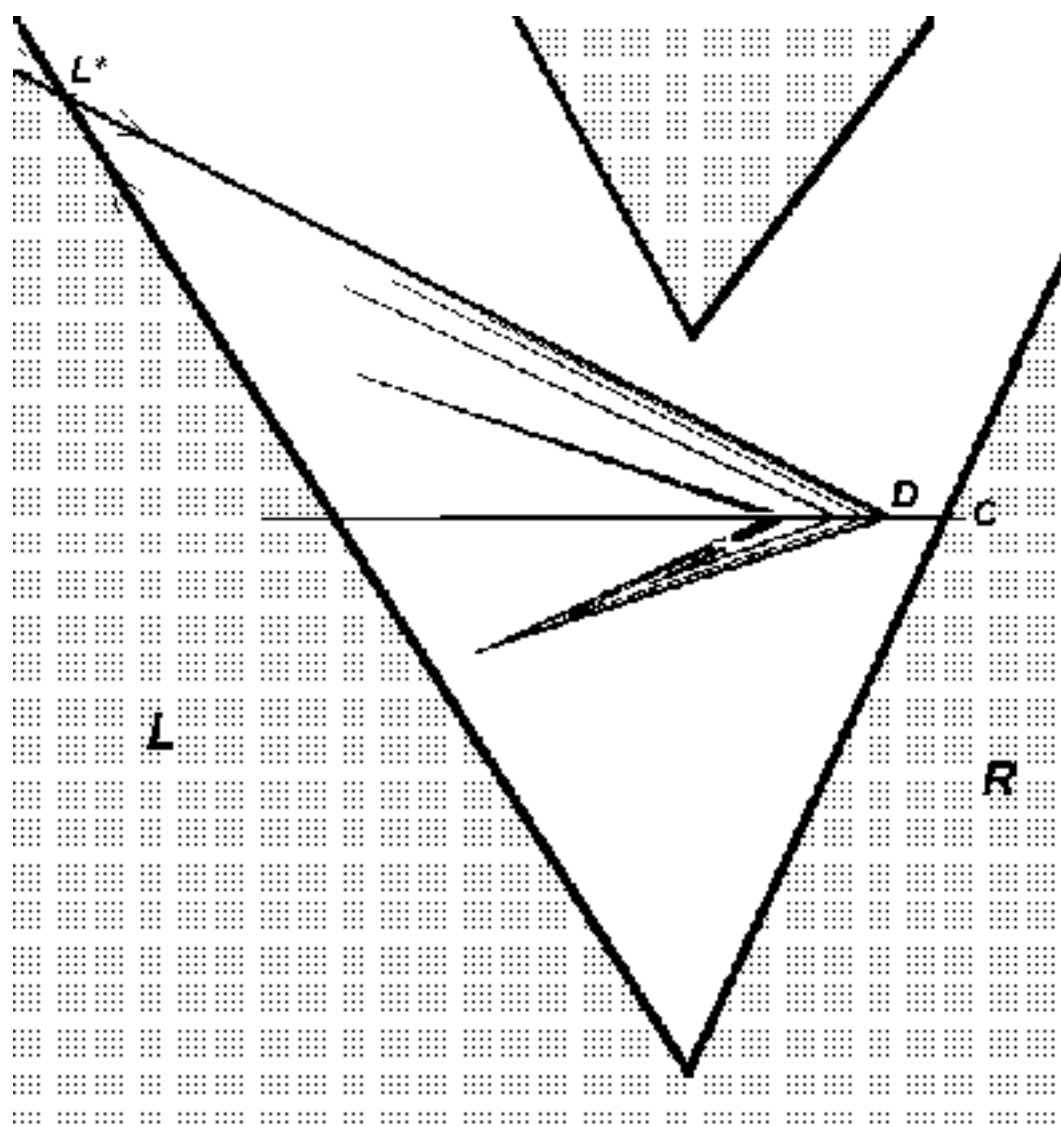


Fig.7



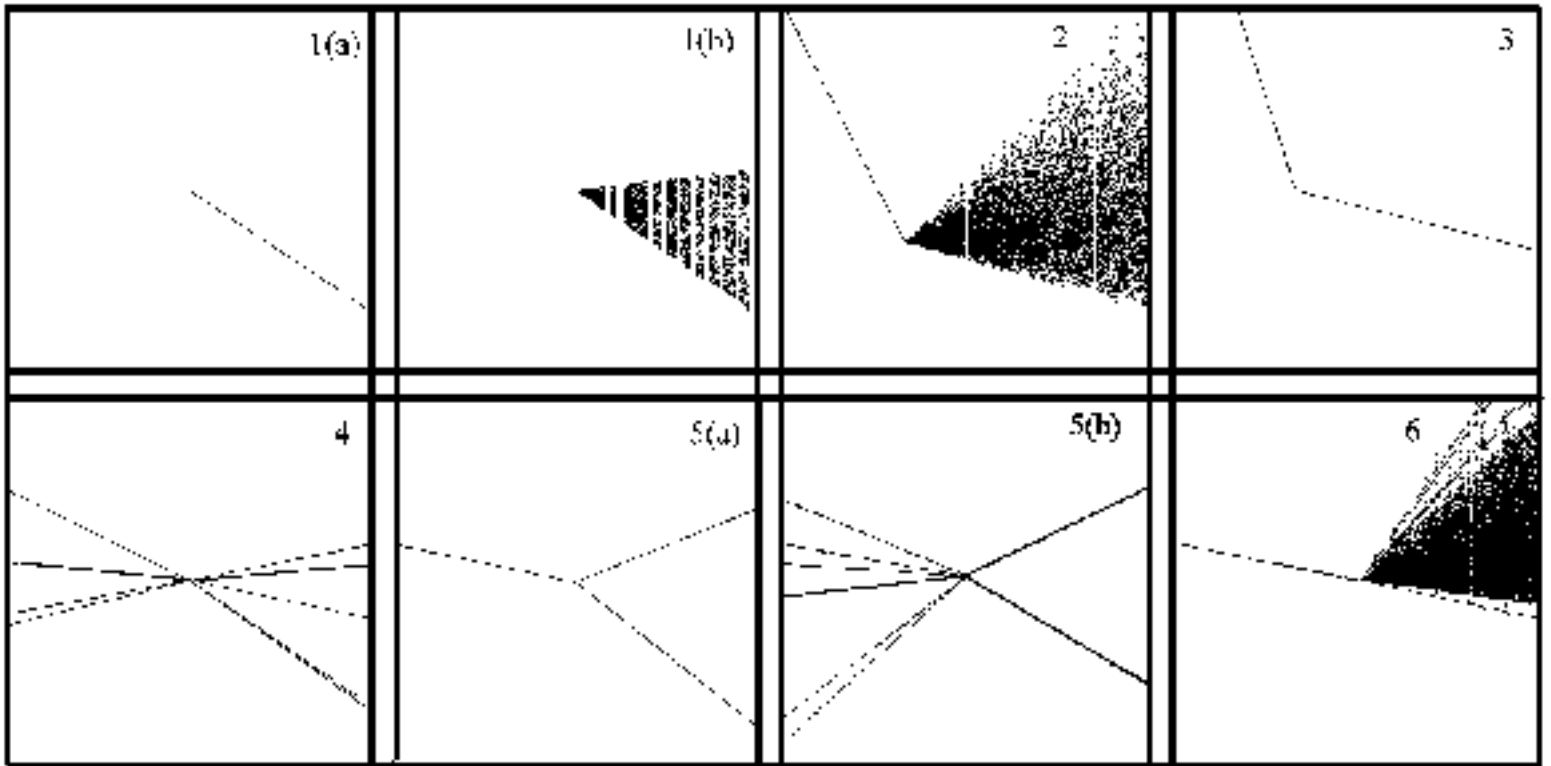


Fig.8

